HHS Public Access

Author manuscript

Cancer Lett. Author manuscript; available in PMC 2020 December 18.

Published in final edited form as:

Cancer Lett. 2016 August 10; 378(2): 97–103. doi:10.1016/j.canlet.2016.05.013.

Carbon ion radiotherapy decreases the impact of tumor heterogeneity on radiation response in experimental prostate tumors

Christin Glowa[1,2,6], **Christian P. Karger**[2,6], **Stephan Brons**[3,6], **Dawen Zhao**[4], **Ralph P. Mason**[4], **Peter E. Huber**[1,5,6], **Jürgen Debus**[1,6], **Peter Peschke**[5,6]

[1]Dept. of Radiation Oncology, University Hospital Heidelberg, Heidelberg, Germany

[2]Dept. of Medical Physics in Radiation Oncology, German Cancer Research Center (DKFZ), Heidelberg, Germany

[3]Heidelberg Ion Beam Therapy Center (HIT), Heidelberg, Germany

[4]Dept. of Radiology, University of Texas Southwestern Medical Center, Dallas, Texas, USA

[5]Dept. of Molecular Radiation Oncology, German Cancer Research Center (DKFZ), Heidelberg, Germany

[6]National Center for Radiation Oncology (NCRO), Heidelberg Institute for Radiation Oncology (HIRO), Heidelberg, Germany

Abstract

Objective: To quantitatively study the impact of intrinsic tumor characteristics and microenvironmental factors on local tumor control after irradiation with carbon (^{12}C-) ions and photons in an experimental prostate tumor model.

Material and Methods: Three sublines of a syngeneic rat prostate tumor (R3327) differing in grading (highly (-H) moderately (-HI) or anaplastic (-AT1)) were irradiated with increasing single doses of either ^{12}C-ions or 6 MV photons in Copenhagen rats. Primary endpoint was local tumor control within 300 days. The relative biological effectiveness (RBE) of ^{12}C-ions was calculated from the dose at 50% tumor control probability (TCD_{50}) of photons and ^{12}C-ions and was correlated with histological, physiological and genetic tumor parameters.

Results: Experimental findings demonstrated that (i) TCD_{50}-values between the three tumor sublines differed less for ^{12}C-ions (23.6 – 32.9 Gy) than for photons (38.2 – 75.7 Gy), (ii) the slope of the dose-response curve for each tumor line was steeper for ^{12}C-ions than for photons,

Corresponding Author Christin Glowa, German Cancer Research Center (DKFZ), Dept. of Medical Physics in Radiation Oncology (E040), Im Neuenheimer Feld 280, 69120 Heidelberg, Germany, Phone: +49-6221-42-2444, FAX: +49-6221-42-2442, c.glowa@dkfz.de.

Conflict of interest: The authors disclose no potential conflicts of interest.

and (iii) the RBE increased with tumor grading from 1.62 ± 0.11 (H) to 2.08 ± 0.13 (HI) to 2.30 ± 0.08 (AT1).

Conclusion: The response to ^{12}C-ions is less dependent on resistance factors as well as on heterogeneity between and within tumor sublines as compared to photons. A clear correlation between decreasing differentiation status and increasing RBE was found. ^{12}C-ions may therefore be a therapeutic option especially in patients with undifferentiated prostate tumors, expressing high resistance against photons.

Keywords

carbon ion radiotherapy; relative biological effectiveness (RBE); tumor heterogeneity; prostate tumor

1. INTRODUCTION

Although radiotherapy with high-energy photons is one of the major treatment strategies for cancer, tumor response is sometimes transient, and therapy may fail due to recurrence of resistant tumor cells. Indeed, tumors are highly dynamic systems expressing morphological and physiological heterogeneity [1]. Clinically, such heterogeneity influences therapeutic responses, especially in radiotherapy leading to rather shallow dose-response curves for tumors. Currently, clinical decisions on the prescribed radiation dose are still population-based rather than individually, mainly because the influence of tumor-associated factors on tumor response is not sufficiently understood.

After initial experience with different ion types in at the Lawrence Berkley Laboratory (USA)[2], carbon (^{12}C-) ion radiotherapy was introduced 1994 in Japan [3, 4] followed by Europe [5] in 1996. The favorable depth-dose profile of ^{12}C-ions (Bragg-peak), together with the highly advanced beam scanning technique allows the dose to be tailored to the tumor, while sparing the surrounding normal tissue [5]. Besides this gain in geometrical accuracy, the higher linear energy transfer (LET) of ^{12}C-ions with its more clustered local energy deposition is believed to be the main reason for the increased efficacy, which is described by the relative biological effectiveness (RBE), using the response to photons as reference.

Resistance against photon therapy is associated with both, intrinsic cellular factors conditioned by the evolutionary capacity of cancer phenotypes and epigenetic parameters, such as the temporal and spatial heterogeneity of the tumor microenvironment caused by dysfunctional blood flow, low pH and hypoxia [6, 7]. Resulting consequences are impairment of the DNA repair machinery, cell-cycle dysregulation, inhibition of cell death pathways and the upregulation of the endogenous cell stress system. In addition, ionizing radiation generates ROS, promotes tumor cell repopulation and exerts proangiogenic effects via the activation of prosurvival signaling cascades [8]. Intrinsic factors (e.g., genetic instability, mutation rate, and epigenetic status) and extrinsic factors (e.g., microenvironmental factors and therapy) that shape intratumor heterogeneity also influence therapeutic responses by creating tumors with a higher diversity of phenotypes for selection.

Many therapies fail to eliminate all tumor cells, and recurrent cells often display greater genetic instability or emerge biological properties that lead to resistance.

As promising clinical results [3, 5] suggest that high-LET particles might overcome classical photon therapy resistance factors, dose-response studies were performed in three experimental prostate tumor sublines differing in grading. The most important finding was that doses required for local tumor control differed significantly and the dose-response curves were steeper for ^{12}C-ions, as compared to photons. As both indicate a minor impact of tumor heterogeneity on therapy outcome after ^{12}C-ion therapy, dose-response parameters were correlated with known resistance factors like undifferentiation, hypoxia, vessel maturity and stem cell content.

2. MATERIAL AND METHODS

2.1 Tumor model

Fresh fragments of tumor tissue of the syngeneic Dunning prostate adenocarcinoma sublines R3327-H, -HI and -AT1 [9] were implanted subcutaneously in the distal right thigh of young adult male Copenhagen rats (weight 180–200 g, Charles River Laboratories Inc., Wilmington, Massachusetts, USA). All experiments were approved by the governmental review committee on animal care, and animals were kept under standard laboratory conditions. During irradiation of H- and HI-tumors, rats were kept under inhalation anesthesia with a mixture of 2.5% sevoflurane (Abbott, Wiesbaden, Germany) and oxygen at 2 l/min using an inhalation mask. In AT1-irradiation studies animals were anesthetized with an intraperitoneal injection of Ketamine hydrochloride (125 mg/kg, Pfizer Deutschland GmbH, Berlin, Germany) mixed with Xylazine hydrochloride (20 mg/kg, Bayer HealthCare AG, Leverkusen, Germany) and breathed air [10].

2.2 Irradiation setup

The experimental setup is essentially the same as previously published [10, 11]. Rats were placed in a special device for accurate positioning of the tumor (see details in [10]. The mean tumor diameter at treatment was 10.5 mm (range 9.0 to 12.0 mm). Photon irradiations were performed using a single 6 MV beam of a linear accelerator (Siemens, Erlangen, Germany) with a 15 mm diameter at the isocenter (90% isodose). For ^{12}C-ions, the tumor was positioned in the center of a single 20 mm spread-out-Bragg-peak (SOBP) having a field diameter of 16.5 mm (90% isodose). The mean dose-averaged LET in the tumor was 75 keV/μm (range 64 – 96 keV/ μm).

In the present study, 178 animals with H- or HI-tumors were irradiated with increasing single doses of photons or ^{12}C-ions, respectively (Table I). 36 sham-treated animals served as controls. Primary endpoint was local tumor control within 300 days, defined as no detectable tumor regrowth. Tumor volume was measured routinely using a caliper. As some tumors showed recurrences near to 300 days, the actual observation time exceeded 300 days and in case of regrowth, the interpolated starting point of regrowth was used to decide whether the tumor was controlled.

For the HI-tumor three recurrences occurred after 300, but within 320 days. Therefore, local control within 320 days was used as secondary endpoint for this tumor. While locally controlled AT1- and HI-tumors regressed completely, residual fibrotic nodules remained in case of locally controlled H-tumors. These nodules were extracted and investigated histologically for fibrotic pattern (Hematoxylin / Eosin) and proliferation (BrdU). A fibrotic pattern without proliferation was considered as secondary endpoint for locally controlled H-tumors (Supplementary Fig. S1).

2.3 Dose response analysis

For the endpoint “local tumor control”, actuarial control rates were calculated and the logistic dose-response model was fitted using the maximum likelihood fitting procedure of the software STATISTICA (version 10.0, Statsoft Inc., www.statsoft.com) (see [10, 11] for details). Incomplete follow-up of animals was considered in the fitting procedure using the method of effective sample sizes that corrects the number of treated and responding tumors to match actuarial response rates and their variances [12]. For the endpoint “histological tumor control”, no actuarial approach was required as surviving (i.e. proliferating) tumor cells were directly detected. In this case the dose-response model was adjusted to the experimentally observed incident rates determined for this endpoint. For all endpoints, the RBE was calculated as the ratio of the TCD_{50}-values (dose at 50% tumor control probability) for photons and ^{12}C-ions. As the results showed a clear dependence on tumor grading, we further analyzed tumor-associated factors in untreated tumors in separate experiments to identify potential underlying causes.

2.4 Histopathology

For evaluation of the differentiation status, Hematoxylin / Eosin staining (Carl Roth GmbH & Co. KG, Karlsruhe, Germany) of cryo-preserved- or paraffin-embedded tissue was performed (see Supplement).

2.5 Immunohistochemistry

Cryo-preserved methanol/acetone fixed tissue was stained for proliferating cells using a BrdU antibody (Roche Diagnostics, Mannheim, Germany). Prior to sacrifice, BrdU (100 mg/kg, Sigma-Aldrich, Taufkirchen, Germany) was injected intraperitoneally. Depending on the proliferation rate of the tumors, BrdU circulation time was 16 h for H-, 8 h for HI-, and 4 h for AT1-tumors. To detect hypoxic areas in tumors, 60 mg/kg pimonidazole (Hypoxyprobe™−1, NPI, Inc., Burlington, MA, USA) was injected intravenously 1 h before sacrificing. Cell nuclei were counterstained with DAPI (Invitrogen Molecular Probes, Eugene, USA). Vascular structures (mouse anti-rat CD31-antibody (Chemicon-Merck-Millipore, Billerica, MA, USA) and pericytes (rabbit anti-SMA (Abcam, Cambridge, UK) were double stained and visualized using fluorochrom-labelled antibodies (see Supplement).

2.6 Magnetic resonance imaging (MRI)

Regional tumor oxygen tension was measured by MRI (Omega CSI4.7; Bruker BioSpin Corporation, Fremont, CA, USA) in untreated tumors at volumes of about 1 cm^3, while rats breathed air (AT1) or oxygen (H, HI) using ^{19}F-pulse burst saturation recovery (FREDOM)

of the reporter molecule hexafluorobenzene, deposited at individual locations, in both central and peripheral regions, as described previously [13] and detailed in the Supplementary material.

2.7 Statistics

Standard errors of TCD_{50} and RBE were calculated by error propagation. For TCD_{50}, the correlation of the fit parameters was considered. In addition, 90% confidence intervals (CIs) were calculated using Fieller's theorem [14]. The differences of the model-based estimates of TCD_{50} and RBE between experimental arms were tested for significance by comparing the ratio of the difference and the propagated standard error with the quantiles of a normal distribution. Differences in the histological parameters between tumor sublines were tested using the two-sided Mann-Whitney U test for independent samples as the Shapiro-Wilk test revealed significant deviations from normal distribution for some of the underlying data. Values of $p<0.05$ and $p<0.0005$ were considered as significant and highly significant, respectively.

3. RESULTS

3.1 Dose-response

Figure 1 shows the adjusted dose-response curves for tumors of the three tumor sublines and all endpoints. The corresponding TCD_{50}- and RBE-values are given in Table II. Mean tumor regression (complete tumor volume reduction) times for the H-, HI- and AT1-tumor were ≥300 d, 42 ± 1.7 d and 110 ± 4.7 d for photons, and ≥300 d, 44 ± 1.7 d and 80 ± 2.0 d for ^{12}C-ions, respectively. While locally controlled AT1- and HI-tumors regressed completely, tiny nodules remained in case of locally controlled H-tumors. As the H-tumors exhibit very long volume doubling times, treatment response was protracted as well and recurrences beyond the 300 day follow-up could not be ruled-out, even if no indication of regrowth was seen within this period. Using lack of proliferative activity together with a fibrotic pattern as secondary histological endpoint, the dose-response curves (Fig. 1 dotted line) were shifted markedly by 10.1 Gy for photons and only 3.2 Gy for ^{12}C-ions (TCD_{50}).

Three important findings can be derived from the dose-response study: (i) as quantified by the TCD_{50}values (Fig. 2A), the dose-response curves for all three tumor sublines (Fig. 1) were located much closer to each other for ^{12}C-ions (23.6 – 32.9 Gy) than for photons (38.2 – 75.7 Gy), (ii) the slope of the dose-response curve (Fig. 2B) for each subline was steeper for ^{12}C-ions than for photons, and (iii) the RBE increased with tumor grading (i.e. H vs. HI vs. AT1), independent of the considered endpoint (Fig. 2C). This RBE-increase is a direct consequence of the fact that the increase of TCD_{50} with tumor grading is much stronger for photons than for ^{12}C-ions.

3.2 Characterization of sublines

HE-stained histological sections of H-, HI-, and AT1-tumors exhibited marked phenotypical differences (Fig. 3A–C). H-tumors showed high stromal density and tubular structures similar to those found in normal prostate tissues. In contrast, HI-tumors tended to form irregular ring-like structures filled with large amounts of mucin, and AT1-tumors were found

to be anaplastic without tubular structures. Thus, glandular differentiation was associated with slow tumor growth. Structural-functional characteristics of the three untreated tumor sublines are summarized in Fig. 3 and Table III. Proliferation, measured as volume doubling time, decreased from 20 days for the well differentiated H- to 5 days for the anaplastic AT1-tumor (Fig. 3D–F, Table III). For the HI-tumor both, the level of differentiation as well as the volume doubling time were intermediate. Typical for the H-tumors was a rather mature vasculature with prominent pericytes (Fig. 3G), associated with a high blood perfusion and little to no hypoxia (Fig. 3J), and a rather broad distribution of pO_2-values. HI-tumors, although showing highest amount of $CD31^+$ vascular structures with an appropriate diameter, were characterized by a lack of pericytes (Fig. 3H). Nevertheless, these tumors were well perfused with only restricted hypoxic regions (Fig. 3K), also depicted by a narrower pO_2-distribution in the histogram (Fig. 3N). In contrast, few peripheral mature vessels and many small immature capillaries in central regions are the cause for extensive chronic hypoxia in AT1-tumors (Table III, Fig. 3L). Ploidy patterns, analyzed by flow-cytometry appeared characteristic for each subline. While the two better differentiated HI- and H-tumors contained a prominent subpopulation of peridiploid cells with a DNA-labeling index of 1.07 and an aneuploidic cell fraction with a concordant DNA-index of 1.8, the AT1-tumor was characterized by a high amount of aneuploidic cells in the near tetraploid range (Table III). In a semi-quantitative double staining approach, expression patterns of putative stem cell surface markers ($CD24^+/CD44^+/CD133^+/CD326^+$) correlate with tumor grading inasmuch as the number of positive cells increase with a higher amount of genomic alterations.

4. DISCUSSION

In the present study, a decreased dependence on tumor grading and steeper dose-response curves for ^{12}C-ions were found. Consequently, the RBE increased significantly with tumor grading. While non-controlled anaplastic AT1-tumors [11] recurred within 180 days, some HI-tumors showed regrowth around day 300. Extending the follow-up time, however, had no significant influence on TCD_{50} and RBE (Table II) and hence, the RBE at 300 days is considered as reliable. The extremely slow turnover of the differentiated H-tumor, with its occasionally remaining tissue nodules caused a less distinct tumor status at 300 days. We therefore used lack of proliferative activity within these nodules as secondary but still growth-related endpoint. Although the respective TCD_{50}-values increased for both, photons and ^{12}C-ions, the RBE differed only non-significantly from that of the primary endpoint local control. The local control-based RBE of the H-Tumor can therefore be considered as reliable.

The increase of RBE with tumor grading (Fig. 2C) is primarily caused by a significantly higher radiation resistance against photons of the less differentiated tumor sublines, while the tolerance against ^{12}C-ions remains much less affected (Fig. 2A). It has to be noted that although the TCD_{50}-values still differ significantly (marginally for AT1 vs. HI and highly for AT1 and HI vs. H) for ^{12}C-ions, the differences are quantitatively much smaller than for photons. In addition, the dose-response curves for the same tumor were generally steeper for ^{12}C-ions than for photons (Fig. 2B), indicating that the effectiveness of ^{12}C-ions is less

dependent on biological heterogeneity not only between sublines, but also within tumors of the same subline.

Transferring this result to patients suggests that tumor-specific radioresistance factors, which prevent therapeutic success in photon radiotherapy, can be at least partially overridden by ^{12}C-ions. To elucidate the relative impact of the different resistance factors in ^{12}C-ion therapy as well as to identify possible underlying molecular mechanisms, detailed characterization of tumors prior and after irradiation is required. Although this was beyond the scope of the present study, the compilation of tumor characteristics in Table III presents candidates for these radioresistance factors.

Key biological features governing tumor responses to photon radiation include tumor hypoxia, DNA damage repair, angiogenesis/vasculogenesis, cancer stem cells, tumor stroma, and the immune response pathways. In contrast to *in vitro* studies with cell populations, possessing single defined inherent or acquired photon therapy resistance patterns, it is presently not feasible to fully assess the significance or the contribution of each biological factor to the complex dynamics of therapy resistance *in vivo*, where all factors interact simultaneously.

The rise of therapy resistance to photons from highly differentiated H-tumors to anaplastic AT1-tumors is associated with a significant decrease in p53 [15] together with higher bcl-2-levels in anaplastic AT1-tumors [16]. Prostatic progression is often associated with changes in interactions between the androgen-dependent stromal microenvironment and tumor cells, with loss of smooth muscle cells and appearance of carcinoma-associated fibroblasts [17, 18]. HI- and AT1-tumors exhibit minor requirements for stromal interaction and their malignant stroma may contribute more to maintaining the three-dimensional tumor architecture [19] than to keeping a differentiated tumor phenotype.

Tumor growth and differentiation strongly depend on blood supply, vascularization, and angiogenesis [20]. Accordingly, in the Dunning model, a negative correlation of tumor malignancy with vessel maturity, accompanied by a reduced perfusion and higher levels of interstitial pressure in anaplastic tumors, all powerful triggers of therapy resistance was observed [21]. Both differentiated tumors are normoxic, typically with $pO_2 \geq 52$ Torr and small hypoxic fractions HF_{10} = 1% (H) and 1.3% (HI), especially when animals were breathing oxygen, as in the present study. When rats were breathing air, as in case of experiments with AT1-tumors, extensive signs of hypoxia with pO_2-values around 14 Torr and a hypoxic fraction HF_{10} = 18% are typical. These intratumoral heterogeneities clearly influence the steepness of dose-response curves (Figure 3A–B).

^{12}C-ions induce a higher level of clustered DNA-damage [22], due to a more dense energy deposition within small areas of DNA-sites. The average number of lesions per cluster tends to increase with increasing LET [23] and is considered the most important contributor to the higher effectiveness of ^{12}C-ions [24]. Cellular repair proficiency may also be relevant. Mutant cells, possessing hampered DSB-repair capacity, do not exhibit large RBEs [25], but alterations of DNA-damage processing exhibit minor resistance to ^{12}C-ions [26]. Finally, deregulated cell death pathways, such as survivin and bcl-2 overexpression that protect cells

from apoptosis may account for therapeutic resistance [27]. Although not an absolute requirement, a higher bcl-2 protein expression is clearly associated with the progression to an androgen-independent metastatic phenotype in human tumors [28], as well as in the Dunning system [16]. The more serious damage produced by high-LET radiation might counteract such cell protective features [29, 30].

Compared to photons, the response to ^{12}C-ion treatment generally occurred faster, even in differentiated, slow growing tumors. Hence, radiation resistance mediated via fibroblasts, vascular elements and immunological factors [7], which limit treatment efficacy by providing a protective environment seems to be of minor importance. The role of tumor vasculature is difficult to judge because blood vessels are highly affected by radiotherapy, especially by high single doses [31]. Moreover, evidence emerged that high-LET irradiation enhances apoptosis by activation of Caspase-3 through Caspase-9, even in the presence of mutated p53, raising the idea of two distinct types of cell death [32, 33].

A differential response of resting or slowly cycling cells is another option for the increased effectiveness of ^{12}C-ions. As irradiation preferentially inactivates proliferating cells, it is postulated that tumor recurrence results partly from the regrowth of quiescent tumor cells that could not be sufficiently killed [34]. In contrast, for ^{12}C-ions a more efficient inhibition of recovery in quiescent cells was detected in preclinical experiments [35, 36] and in a clinical study [37].

Finally, subsets of cancer stem cells (CSCs) are assumed to be responsible for radioresistance [38–41]. While in human prostate cancer, the existence of CSCs is a matter of debate, several candidate cell populations were identified in the Dunning system [42]. For selected human tumors a higher radioresistance of CSCs due to either increased activation of DNA-repair or upregulated free radical scavenging systems is described [43, 44]. Proficient DNA-damage and higher intracellular ROS-levels in CSCs, make particles a promising strategy to overcome radioresistance of CSCs [45, 46].

Conclusion

Intrinsic tumor characteristics contributing to radioresistance against photons, have minor impact for high-LET irradiations. Candidates for these resistance factors are DNA-repair capacity, p53-status, cell death regulation, as well as microenvironmental factors. As shown in an experimental prostate model, tumor control by ^{12}C-ions is less dependent on tumor heterogeneity. In case of unclear resistance factors to photons, ^{12}C-ions may therefore provide a therapeutic advantage.

Supplementary Material

Refer to Web version on PubMed Central for supplementary material.

ACKNOWLEDGEMENTS

The authors are grateful to Prof. Eric Hahn for his valuable hints in experiment design, Angela Funk and Marina Szymbara for excellent technical support and the staff of the Heidelberg Ion Therapy Center (HIT) for providing excellent working conditions.

Financial support: This study was supported by Deutsche Forschungsgemeinschaft (DFG, KFO214) and by NIH NCI R01 CA139043, P41 EB015908, and P30 CA142543.

Abbreviations:

^{12}C	carbon ions
LET	linear energy transfer
RBE	relative biological effectiveness
ROS	reactive oxygen species
TCD_{50}	dose at 50% tumor control probability
CI	confidence interval
MRI	magnetic resonance imaging
FREDOM	^{19}F-pulse burst saturation recovery
HF	hypoxic fraction
CSC	cancer stem cells

REFERENCES

[1]. Egeblad M, Nakasone ES, Werb Z, Tumors as organs: complex tissues that interface with the entire organism, Developmental Cell, 18 (2010) 884–901. [PubMed: 20627072]

[2]. Castro JR, Linstadt DE, Bahary JP, Petti PL, Daftari I, Collier JM, Gutin PH, Gauger G, Phillips TL, Experience in charged particle irradiation of tumors of the skull base: 1977–1992, International Journal of Radiation Oncology, Biology, Physics, 29 (1994) 647–655.

[3]. Kamada T, Clinical evidence of particle beam therapy (carbon), International Journal of Clinical Oncology, 17 (2012) 85–88. [PubMed: 22426888]

[4]. Kamada T, Tsujii H, Blakely EA, Debus J, De Neve W, Durante M, Jakel O, Mayer R, Orecchia R, Potter R, Vatnitsky S, Chu WT, Carbon ion radiotherapy in Japan: an assessment of 20 years of clinical experience, The Lancet Oncology, 16 (2015) 93–100.

[5]. Combs SE, Debus J, Treatment with heavy charged particles: systematic review of clinical data and current clinical (comparative) trials, Acta Oncologica, 52 (2013) 1272–1286. [PubMed: 23964656]

[6]. Tatum JL, Kelloff GJ, Gillies RJ, Arbeit JM, Brown JM, Chao KS, Chapman JD, Eckelman WC, Fyles AW, Giaccia AJ, Hill RP, Koch CJ, Krishna MC, Krohn KA, Lewis JS, Mason RP, Melillo G, Padhani AR, Powis G, Rajendran JG, Reba R, Robinson SP, Semenza GL, Swartz HM, Vaupel P, Yang D, Croft B, Hoffman J, Liu G, Stone H, Sullivan D, Hypoxia: importance in tumor biology, noninvasive measurement by imaging, and value of its measurement in the management of cancer therapy, International Journal of Radiation Biology, 82 (2006) 699–757. [PubMed: 17118889]

[7]. Junttila MR, de Sauvage FJ, Influence of tumour micro-environment heterogeneity on therapeutic response, Nature, 501 (2013) 346–354. [PubMed: 24048067]

[8]. Good JS, Harrington KJ, The hallmarks of cancer and the radiation oncologist: updating the 5Rs of radiobiology, Clinical Oncology, 25 (2013) 569–577. [PubMed: 23850153]

[9]. Isaacs JT, Heston WD, Weissman RM, Coffey DS, Animal models of the hormone-sensitive and -insensitive prostatic adenocarcinomas, Dunning R-3327-H, R-3327-HI, and R-3327-AT, Cancer Research, 38 (1978) 4353–4359. [PubMed: 698976]

[10]. Peschke P, Karger CP, Scholz M, Debus J, Huber PE, Relative biological effectiveness of carbon ions for local tumor control of a radioresistant prostate carcinoma in the rat, International Journal of Radiation Oncology, Biology, Physics, 79 (2011) 239–246.

[11]. Karger CP, Peschke P, Scholz M, Huber PE, Debus J, Relative biological effectiveness of carbon ions in a rat prostate carcinoma in vivo: comparison of 1, 2, and 6 fractions, International Journal of Radiation Oncology, Biology, Physics, 86 (2013) 450–455.

[12]. Walker AM, Suit HD, Assessment of local tumor control using censored tumor response data, International Journal of Radiation Oncology, Biology, Physics, 9 (1983) 383–386.

[13]. Zhao D, Jiang L, Mason RP, Measuring changes in tumor oxygenation, Methods in Enzymology, 386 (2004) 378–418. [PubMed: 15120262]

[14]. Finney DJ, Statistical Method in Biological Assay 3rd edition London: Charles Griffin, 1978.

[15]. Cooke DB, Quarmby VE, Mickey DD, Isaacs JT, French FS, Oncogene expression in prostate cancer: Dunning R3327 rat dorsal prostatic adenocarcinoma system, The Prostate, 13 (1988) 263–272. [PubMed: 3217275]

[16]. Furuya Y, Krajewski S, Epstein JI, Reed JC, Isaacs JT, Expression of bcl-2 and the progression of human and rodent prostatic cancers, Clinical Cancer Research, 2 (1996) 389–398. [PubMed: 9816182]

[17]. Arnold JT, Isaacs JT, Mechanisms involved in the progression of androgen-independent prostate cancers: it is not only the cancer cell's fault, Endocrine-related Cancer, 9 (2002) 61–73. [PubMed: 11914183]

[18]. Cunha GR, Hayward SW, Wang YZ, Role of stroma in carcinogenesis of the prostate, Differentiation; Research in Biological Diversity, 70 (2002) 473–485.

[19]. Wang X, An Z, Geller J, Hoffman RM, High-malignancy orthotopic nude mouse model of human prostate cancer LNCaP, The Prostate, 39 (1999) 182–186. [PubMed: 10334107]

[20]. Jain RK, Molecular regulation of vessel maturation, Nature Medicine, 9 (2003) 685–693.

[21]. Zechmann CM, Woenne EC, Brix G, Radzwill N, Ilg M, Bachert P, Peschke P, Kirsch S, Kauczor HU, Delorme S, Semmler W, Kiessling F, Impact of stroma on the growth, microcirculation, and metabolism of experimental prostate tumors, Neoplasia, 9 (2007) 57–67. [PubMed: 17325744]

[22]. Tobias F, Durante M, Taucher-Scholz G, Jakob B, Spatiotemporal analysis of DNA repair using charged particle radiation, Mutation Research, 704 (2010) 54–60. [PubMed: 19944777]

[23]. Georgakilas AG, O'Neill P, Stewart RD, Induction and repair of clustered DNA lesions: what do we know so far?, Radiation Research, 180 (2013) 100–109. [PubMed: 23682596]

[24]. Matsumura S, Matsumura T, Ozeki S, Fukushima S, Yamazaki H, Inoue T, Furusawa Y, Eguchi-Kasai K, Comparative analysis of G2 arrest after irradiation with 75 keV carbon-ion beams and 137Cs gamma-rays in a human lymphoblastoid cell line, Cancer Detection and Prevention, 27 (2003) 222–228. [PubMed: 12787730]

[25]. Weyrather WK, Ritter S, Scholz M, Kraft G, RBE for carbon track-segment irradiation in cell lines of differing repair capacity, International Journal of Radiation Biology, 75 (1999) 1357–1364. [PubMed: 10597910]

[26]. Takahashi T, Fukawa T, Hirayama R, Yoshida Y, Musha A, Furusawa Y, Ando K, Nakano T, In vitro interaction of high-LET heavy-ion irradiation and chemotherapeutic agents in two cell lines with different radiosensitivities and different p53 status, Anticancer Research, 30 (2010) 1961–1967. [PubMed: 20651340]

[27]. Adams JM, Cory S, The Bcl-2 protein family: arbiters of cell survival, Science, 281 (1998) 1322–1326. [PubMed: 9735050]

[28]. Shabaik AS, Krajewski S, Burgan A, Krajewska M, Reed JC, bcl-2 protooncogene expression in normal, hyperplastic, and neoplastic prostate tissue, Journal of Urology and Pathology, 3 (1995) 17–27.

[29]. Jin XD, Gong L, Guo CL, Hao JF, Wei W, Dai ZY, Li Q, Survivin expressions in human hepatoma HepG2 cells exposed to ionizing radiation of different LET, Radiation and Environmental Biophysics, 47 (2008) 399–404. [PubMed: 18340453]

[30]. Hamada N, Hara T, Omura-Minamisawa M, Funayama T, Sakashita T, Sora S, Yokota Y, Nakano T, Kobayashi Y, Energetic heavy ions overcome tumor radioresistance caused by overexpression of Bcl-2, Radiotherapy and Oncology, 89 (2008) 231–236. [PubMed: 18336939]

[31]. Park HJ, Griffin RJ, Hui S, Levitt SH, Song CW, Radiation-induced vascular damage in tumors: implications of vascular damage in ablative hypofractionated radiotherapy (SBRT and SRS), Radiation Research, 177 (2012) 311–327. [PubMed: 22229487]

[32]. Yamakawa N, Takahashi A, Mori E, Imai Y, Furusawa Y, Ohnishi K, Kirita T, Ohnishi T, High LET radiation enhances apoptosis in mutated p53 cancer cells through Caspase-9 activation, Cancer Science, 99 (2008) 1455–1460. [PubMed: 18422753]

[33]. Maalouf M, Alphonse G, Colliaux A, Beuve M, Trajkovic-Bodennec S, Battiston-Montagne P, Testard I, Chapet O, Bajard M, Taucher-Scholz G, Fournier C, Rodriguez-Lafrasse C, Different mechanisms of cell death in radiosensitive and radioresistant p53 mutated head and neck squamous cell carcinoma cell lines exposed to carbon ions and x-rays, International Journal of Radiation Oncology, Biology, Physics, 74 (2009) 200–209.

[34]. Vaupel P, Tumor microenvironmental physiology and its implications for radiation oncology, Seminars in Radiation Oncology, 14 (2004) 198–206. [PubMed: 15254862]

[35]. Hirayama R, Furusawa Y, Fukawa T, Ando K, Repair kinetics of DNA-DSB induced by X-rays or carbon ions under oxic and hypoxic conditions, Journal of Radiation Research, 46 (2005) 325–332. [PubMed: 16210789]

[36]. Staab A, Zukowski D, Walenta S, Scholz M, Mueller-Klieser W, Response of Chinese hamster v79 multicellular spheroids exposed to high-energy carbon ions, Radiation Research, 161 (2004) 219–227. [PubMed: 14731067]

[37]. Nakano T, Suzuki Y, Ohno T, Kato S, Suzuki M, Morita S, Sato S, Oka K, Tsujii H, Carbon beam therapy overcomes the radiation resistance of uterine cervical cancer originating from hypoxia, Clinical Cancer Research, 12 (2006) 2185–2190. [PubMed: 16609033]

[38]. Baumann M, Krause M, Hill R, Exploring the role of cancer stem cells in radioresistance, Nature reviews. Cancer, 8 (2008) 545–554. [PubMed: 18511937]

[39]. Krause M, Yaromina A, Eicheler W, Koch U, Baumann M, Cancer stem cells: targets and potential biomarkers for radiotherapy, Clinical Cancer Research, 17 (2011) 7224–7229. [PubMed: 21976536]

[40]. Rich JN, Cancer stem cells in radiation resistance, Cancer Research, 67 (2007) 8980–8984. [PubMed: 17908997]

[41]. Hill RP, Marie-Egyptienne DT, Hedley DW, Cancer stem cells, hypoxia and metastasis, Seminars in Radiation Oncology, 19 (2009) 106–111. [PubMed: 19249648]

[42]. Glowa C, Peschke P, Karger CP, Hahn EW, Huber PE, Debus J, Ehemann V, Flow cytometric characterization of tumor subpopulations in three sublines of the dunning R3327 rat prostate tumor model, The Prostate, 73 (2013) 1710–1720. [PubMed: 23853045]

[43]. Bao S, Wu Q, McLendon RE, Hao Y, Shi Q, Hjelmeland AB, Dewhirst MW, Bigner DD, Rich JN, Glioma stem cells promote radioresistance by preferential activation of the DNA damage response, Nature, 444 (2006) 756–760. [PubMed: 17051156]

[44]. Diehn M, Cho RW, Lobo NA, Kalisky T, Dorie MJ, Kulp AN, Qian D, Lam JS, Ailles LE, Wong M, Joshua B, Kaplan MJ, Wapnir I, Dirbas FM, Somlo G, Garberoglio C, Paz B, Shen J, Lau SK, Quake SR, Brown JM, Weissman IL, Clarke MF, Association of reactive oxygen species levels and radioresistance in cancer stem cells, Nature, 458 (2009) 780–783. [PubMed: 19194462]

[45]. Cui X, Oonishi K, Tsujii H, Yasuda T, Matsumoto Y, Furusawa Y, Akashi M, Kamada T, Okayasu R, Effects of carbon ion beam on putative colon cancer stem cells and its comparison with X-rays, Cancer Research, 71 (2011) 3676–3687. [PubMed: 21454414]

[46]. Laurent C, Leduc A, Pottier I, Prevost V, Sichel F, Lefaix JL, Dramatic increase in oxidative stress in carbon-irradiated normal human skin fibroblasts, PloS One, 8 (2013) e85158.

HIGHLIGHTS

- Compared to the same photon dose, carbon ions are generally more effective.
- In tumors, the effect of carbon ions relative to photons increases with grading.
- Therapeutic response to carbon ion therapy is less heterogeneous than for photons.
- Carbon ions override most conventional tumor-associated factors of radioresistance.

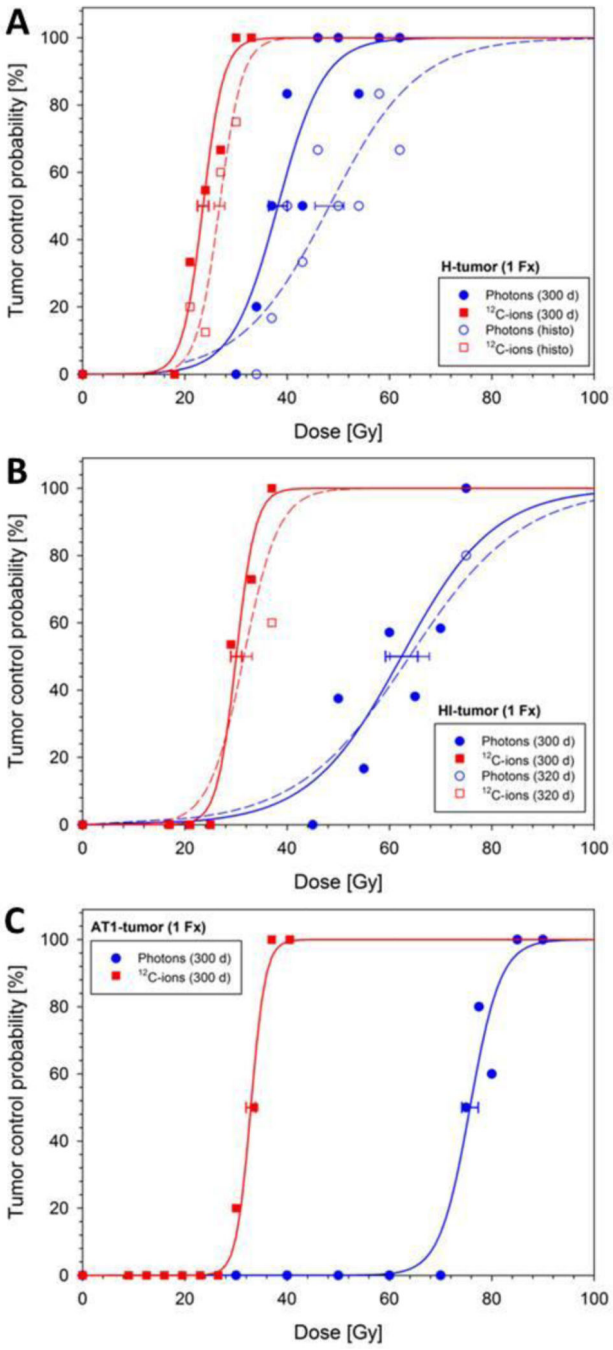

Figure 1:

Dose-response curves of three sublines of the R3327 prostate carcinoma after single fractions of photons and ^{12}C-ions, respectively. The uncertainty (1 SE) of TCD_{50} is indicated. Solid lines refer to the primary endpoint “local tumor control within 300 d”. As additional endpoints “histological tumor control” (H-tumor, A) and “local control within 320 d” (HI-tumor, B) were used. For comparison, the previously measured dose-response curves for the AT1-tumor (C) [11] are also displayed.

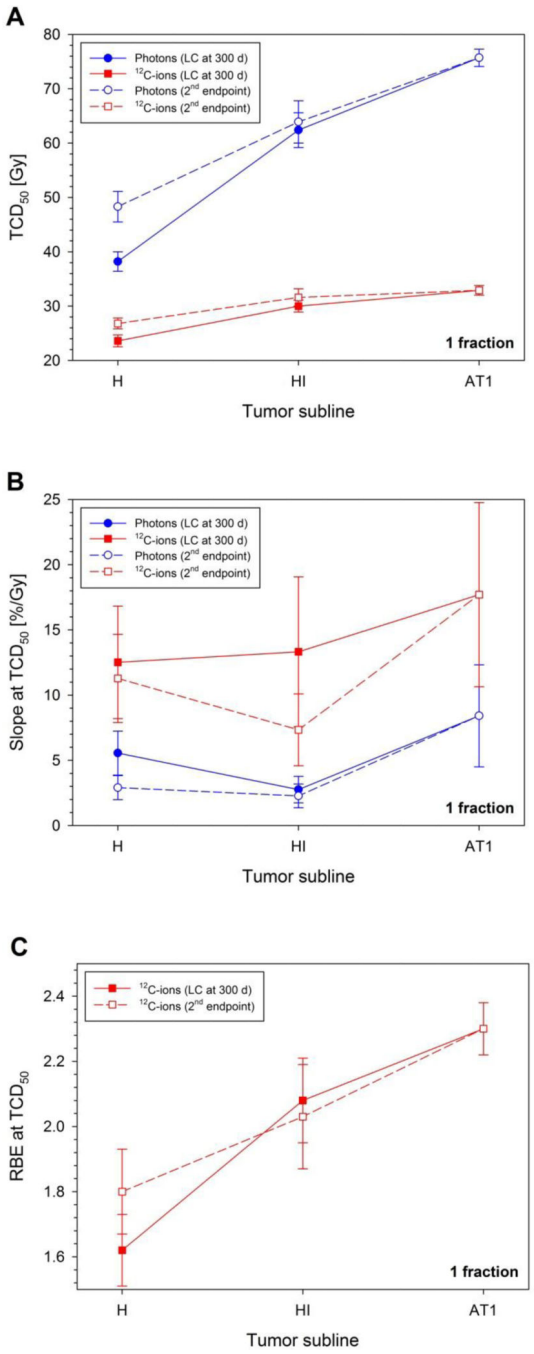

Figure 2:

Dependence of the dose-response parameters for photons and ^{12}C-ions on the tumor subline: The increase of radiation tolerance with increasing tumor grading is stronger for photons than for ^{12}C-ions (A). For a given tumor grading, the slope of the dose-response curve is steeper for ^{12}C-ions than for photons (B). The effectiveness of ^{12}C-ions relative to photons increases with increasing tumor grade (C). These results are essentially independent of uncertainties resulting from the endpoint definition.

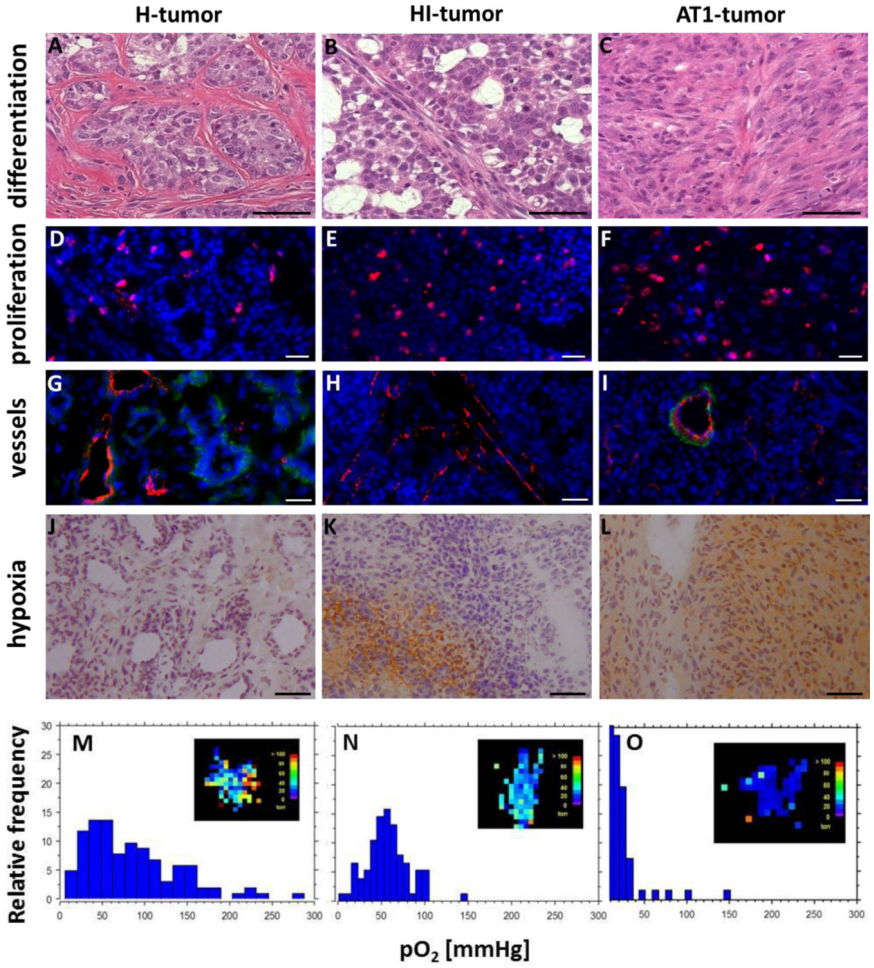

Figure 3:

Comparison of H- (A,D,G,J,M), HI- (B,E,H,K,N) and AT1-tumors (C,F,I,L,O). Structural changes and the differentiation status are detected by Hematoxylin / Eosin (HE) staining (A-C). Proliferating cells were BrdU-labelled (red, D-F) and cell nuclei counterstained with DAPI (blue, D-I). Vessel diameter, structure and maturity were evaluated by staining endothelial cells with CD31 (red) and smooth muscle actin (SMA, green, G-I). For visualization of hypoxic areas pimonidazole was used (brown, J-L). Magnification: 200x; Scale bars: 50 μm. Quantitative MRI-measurements of the oxygen concentration (FREDOM) were used to determine pO_2-maps (M-O, inlets). For a representative tumor of each subline, pO_2-values were converted to histograms.

Table I:

Dose levels and number of animals in the experiment.

Experiment	Dose levels [Gy] (animals per dose level)	Animals
H-Tumor		
Photons	30 (3), 34 (5), 37 (6), 40 (6), 43 (6), 46 (6), 50 (5 *), 54 (6), 58 (6), 62 (3)	52
^{12}C-ions	18 (6), 21 (6 *), 24 (8), 27 (7 **), 30 (9 *), 33 (7 *)	43
Controls	8 sham-treated tumors per experimental arm	16
HI-Tumor		
Photons	45 (4), 50 (8), 55 (6), 60 (7), 65 (7), 70 (8), 75 (7 +)	47
^{12}C-ions	17 (3), 21 (6), 25 (6), 29 (7), 33 (8), 37 (6 ++)	36
Controls	10 sham-treated tumors per experimental arm	20
Total		**214**

*No histology in one animal

**No histology in two animals

+Recurrent tumor in one animal at 305 d

++Recurrent tumor in two animals at 308 d and 320 d, respectively

Table II:

TCD_{50}-and RBE-values for three tumor sublines of the R3327 prostate carcinoma measured in this and a previous study [11].

Endpoint	TCD_{50} ± SE *(90% CI)* [Gy]		RBE ± SE *(90% CI)*
	Photons*	^{12}C-ions*	
H-Tumor (this study)			
LC (300 d)	338.2 ± 1.8 *(34.0 – 41.1)* §	23.6 ± 1.1 *(21.5 – 25.8)*	1.62 ± 0.11 *(1.45 – 1.81)*
Histo†	48.3 ± 2.8 *(43.6 – 54.6)*	26.8 ± 1.0 *(24.9 – 28.8)*	1.80 ± 0.13 *(1.60 – 2.02)*
HI-Tumor (this study)			
LC (300 d)	62.4 ± 3.2 *(56.6 – 69.8)* §	30.0 ± 1.1 *(27.5 – 32.6)* $	2.08 ± 0.13 *(1.87 – 2.30)* &
LC (320 d)‡	63.9 ± 3.9 *(57.5 – 74.7)*	31.6 ± 1.6 *(28.7 – 35.5)*	2.03 ± 0.16 *(1.78 – 2.30)*
AT1-Tumor [11]			
LC (300 d)	75.7 ± 1.6 *(69.9 – 78.6)* §	32.9 ± 0.9 *(30.8 – 34.9)* $	2.30 ± 0.08 *(2.17 – 2.44)* &

Uncertainties are given as single standard errors and 90%-confidence intervals. Endpoints for this dose-response study were “local tumor control (LC) within 300 d or 320 d” or “histological tumor control” (Histo).

*All differences in TCD_{50} between photons and ^{12}C-ions for the same tumor and endpoint are highly significant ($p<0.0005$).

§All differences in TCD_{50} at LC (300 d) between tumor sublines are highly significant ($p<0.0005$).

$Differences in TCD_{50} at LC (300 d) relative to the H-tumor are highly significant ($p<0.0005$), but only significant ($p<0.05$) for HI vs AT1.

&Differences in RBE at LC (300 d) relative to the H-tumor are highly significant ($p<0.0005$) for the AT1- and significant ($p<0.05$) for the HI-tumor.

†Difference relative to LC (300 d) is significant ($p<0.05$) for TCD_{50}-values, but not for the RBE.

‡No significant difference for TCD_{50} and RBE relative to LC (300 d)

Table III:

Resistance factors in the three sublines of the R3327 prostate tumor model.

Heterogeneity factors	H-tumor	HI-tumor	AT1-tumor
Volume doubling time	≈20 days	≈10 days	≈5 days
Vascularization	Many big mature vessels	Big immature vessels	Less vessels, mostly immature
Number of $CD31^+$-vessels	18.35 ± 0.85	22.93 ± 1.91 *	17.31 ± 1.43
Vessel diameter [µm]	14.13 ± 0.26	14.14 ± 0.46	9.07 ± 0.28 §
$CD31^+$-area [%]	2.17 ± 0.23	4.06 ± 0.62 $^$$	2.45 ± 0.32
SMA^+-area [%]	0.71 ± 0.11	0.01 ± 0.01 $^&$	0.34 ± 0.07
Amplitude weighted pO_2 [torr]	136.0 †	52.0 †	14.0 $^#$
Hypoxic fraction [pO_2 < 10 mmHg, HF_{10}]	1 %	1.3 %	18 %
Subpopulations ‡: aneuploidic cells	Diploid (DI 1.0: 33.5%), peridiploid (DI 1.07: 59.1%), hypotetraploid (DI 1.8: 7.3%)	Diploid (DI 1.0: 15.3%), peridiploid (DI 1.07: 82.2%), hypotetraploid (DI 1.8: 2.5%)	Diploid (DI 1.0: 66.5%), hypotetraploid (DI 1.8: 33.5%)
Subpopulations ‡: potential stem cell marker (CD24, CD44, CD133, CD326)	2.9 – 8.0 % of cells	6.6 – 20.3 % of cells	15.3 – 24.6 % of cells

CD31− and SMA-staining are expressed in values ± SE. The amount of vessels was calculated as absolute number of $CD31^+$-vessels per microscopic image (200x magnification). Aneuploidic tumor cells and potential stem cell markers were characterized by flow-cytometry.

*Significant ($p<0.05$) relative to H- and AT1-tumor

§Highly significant ($p<0.0005$) relative to H- and HI-tumor

$^$$Highly significant ($p<0.0005$) relative to H- and significant relative to AT1-tumor

$^&$Highly significant ($p<0.0005$) relative to H- and AT1-tumor

‡DI: DNA-index, values cited from [42]

†Animals breathing oxygen

$^#$Animals breathing air